

## Article

# Absolute Contribution of the Non-Uniform Spatial Distribution of Atmospheric CO<sub>2</sub> to Net Primary Production through CO<sub>2</sub>-Radiative Forcing

Jing Peng <sup>1,\*</sup> , Li Dan <sup>1</sup>, Jinming Feng <sup>1</sup>, Kairan Ying <sup>1</sup>, Xiba Tang <sup>2</sup> and Fuqiang Yang <sup>1</sup> 

<sup>1</sup> CAS Key Laboratory of Regional Climate-Environment for Temperate East Asia, Institute of Atmospheric Physics, Chinese Academy of Sciences, Beijing 100029, China; danli@tea.ac.cn (L.D.); fengjm@tea.ac.cn (J.F.); yingkr@tea.ac.cn (K.Y.); yangfq@tea.ac.cn (F.Y.)

<sup>2</sup> Laboratory of Cloud-Precipitation Physics and Severe Storms (LACS), Institute of Atmospheric Physics, Beijing 100029, China; tangxb\_6@mail.iap.ac.cn

\* Correspondence: pengjing@tea.ac.cn

**Abstract:** Atmospheric concentrations of CO<sub>2</sub> are the most important driver of the Earth's climate and ecosystems through CO<sub>2</sub>-radiative forcing, fueling the surface temperature and latent heat flux on half-century timescales. We used FGOALS-s2 coupled with AVIM2 to estimate the response of net primary production (NPP) to spatial variations in CO<sub>2</sub> during the time period 1956–2005. We investigated how the induced variations in surface temperature and soil moisture influence NPP and the feedback of the oceans and sea ice on changes in NPP. The spatial variations in the concentrations of CO<sub>2</sub> resulted in a decrease in NPP from 1956 to 2005 when we included ocean and sea ice dynamics, but a slight increase in NPP without ocean and sea ice dynamics. One of the reasons is that the positive feedback of sea temperature to the surface temperature leads to a significant decrease in tropical NPP. Globally, the non-uniform spatial distribution of CO<sub>2</sub> absolutely contributed about 14.3% ± 2.2% to the terrestrial NPP when we included ocean and sea ice dynamics or about 11.5% ± 1.1% without ocean and sea ice dynamics. Our findings suggest that more attention should be paid to the response of NPP to spatial variations in atmospheric CO<sub>2</sub> through CO<sub>2</sub>-radiative forcing, particularly at low latitudes, to better constrain the predicted carbon flux under current and future conditions. We also highlight the fundamental importance of changes in soil moisture in determining the pattern, response and magnitude of NPP to the non-uniform spatial distribution of CO<sub>2</sub> under a warming climate.



**Citation:** Peng, J.; Dan, L.; Feng, J.; Ying, K.; Tang, X.; Yang, F. Absolute Contribution of the Non-Uniform Spatial Distribution of Atmospheric CO<sub>2</sub> to Net Primary Production through CO<sub>2</sub>-Radiative Forcing. *Sustainability* **2021**, *13*, 10897. <https://doi.org/10.3390/su131910897>

Academic Editor: Baojie He

Received: 12 August 2021

Accepted: 8 September 2021

Published: 30 September 2021

**Keywords:** non-uniform CO<sub>2</sub>; CO<sub>2</sub>-radiative forcing; net primary production; surface temperature; soil moisture; sea surface temperature

**Publisher's Note:** MDPI stays neutral with regard to jurisdictional claims in published maps and institutional affiliations.



**Copyright:** © 2021 by the authors. Licensee MDPI, Basel, Switzerland. This article is an open access article distributed under the terms and conditions of the Creative Commons Attribution (CC BY) license (<https://creativecommons.org/licenses/by/4.0/>).

## 1. Introduction

Atmospheric CO<sub>2</sub> concentrations are one of the most important drivers of climate in earth system models [1,2]. It can affect the global average surface temperature, the global water cycle, global sea-levels, the loss of Arctic sea ice and the atmospheric vapor pressure deficit through radiative forcing [3–5]. Changes in CO<sub>2</sub> concentrations indirectly affect the growth of land plants and the productivity of terrestrial vegetation (gross primary production) [6]—for example, the gross primary production of terrestrial vegetation decreased after the late 1990s as a result of the increased vapor pressure deficit [5].

There is large uncertainty in the magnitude and spatial distribution of the radiative effect of atmospheric CO<sub>2</sub> concentration (±20%) based on multi-model simulations [7,8]. These models come from the fifth stage of the coupled model comparison project (CMIP5) [9] using the uniformity of atmospheric CO<sub>2</sub> concentration without spatial varying. Although the spatial heterogeneity of atmospheric CO<sub>2</sub> concentrations varies widely on a regional scale [10,11], the contribution of spatially non-uniform CO<sub>2</sub> to the Earth's climate and the terrestrial carbon cycle through CO<sub>2</sub>-radiative forcing is largely unknown [12].

Several studies have reported the impacts of varying atmospheric CO<sub>2</sub> concentrations directly through CO<sub>2</sub>-radiative forcing on climate state [13,14]. Furthermore, it can also disturb the carbon balance [15] and accumulation of carbon on land [16]. For instance, the variations in surface temperature, precipitation and soil moisture [17] influence the rate of photosynthesis and limit net primary production (NPP) and soil respiration [15]. Thus, changes in the Earth's climate through CO<sub>2</sub>-radiative forcing therefore constrain the processes of the carbon cycle [2].

However, predictions of the rise in temperature under historical conditions remain highly uncertain, ranging from about 0.4 to 1.3 °C, mainly due to historical radiative forcing of greenhouse gases [18]. One of the uncertainties results from the lack of a clear understanding about the feedback of spatial variations in atmospheric CO<sub>2</sub> and the lack of reliable measurements of this process in the field. Modeling approaches are therefore vital to constrain climate variables and the carbon fluxes resulting from the spatial varying of CO<sub>2</sub> concentration.

On the other hand, most conventional methodologies do not consider the influence of spatial varying of CO<sub>2</sub> concentrations on the Earth's climate system and biogeochemical cycles. We would focus to quantify the response of terrestrial NPP to the spatial varying of CO<sub>2</sub> concentration through CO<sub>2</sub>-radiative forcing. To further assess the significance of the non-uniform spatial distribution of CO<sub>2</sub> on NPP, we compared simulations with fully coupled atmosphere–land–ocean–sea ice components (simulation A) and coupled atmosphere–land components (simulation B) in the Flexible Global Ocean–Atmosphere–Land System Model Spectral Version 2 (FGOALS-s2) [19] coupled with the Atmosphere–Vegetation Interaction Model (AVIM) [20]. Specifically, we evaluated NPP in FGOALS-AVIM with the implementation of these two different simulations forced by a uniform or non-uniform spatial distribution of atmospheric CO<sub>2</sub> with or without active ocean and sea ice during the time period 1956–2005. We addressed three principal questions: (1) how much does the climate-driven feedback caused by the non-uniform spatial distribution of CO<sub>2</sub> through CO<sub>2</sub>-radiative forcing affect climate variables and NPP; (2) how does the estimated NPP with and without ocean and sea ice dynamics differ as a result of the non-uniform spatial distribution of CO<sub>2</sub> through the radiative forcing associated with spatial variations in the climate variables; and (3) what are the implications of a non-uniform spatial distribution of CO<sub>2</sub> on the global NPP during the time period 1956–2005.

## 2. Methods and Simulations

The Student's *t*-test used in this study is used to estimate of the statistical significance between the variables from different simulations, which are calculated as follows:

$$t_i = \frac{\bar{x}_i - \bar{y}_i}{S_{Pi} \sqrt{\frac{1}{n_1} + \frac{1}{n_2}}} \quad (1)$$

where  $\bar{x}_i$  or  $\bar{y}_i$  is the averaged NPP from simulations with spatial varying of CO<sub>2</sub> concentration or without spatial varying of CO<sub>2</sub> concentration of the *i*-th grid cell during 1956–2005,  $S_{Pi}$  is the weighted average of the standard deviations of NPP from the two simulations during the same period in the *i*-th grid cell.  $n_1$  or  $n_2$  is the equivalent sample sizes of two simulations.

Based on the absolute contribution of each region (each grid cell or PFT) to global NPP, we further classify global NPP into different categories (Figure 1). To this end, we adopted an index to score each geographic location based on consistency. The magnitude of the absolute change in local NPP flux relative to the global NPP under CO<sub>2</sub> uniform distribution was calculated as the following, which was also estimated by [21]:

$$C_j = \frac{\sum_{t=1}^n |\Delta NPP_{jt}|}{\sum_{t=1}^n NPP_t} \quad (2)$$

where  $|\Delta NPP_{jt}|$  is the absolute change in NPP caused by the non-uniform spatial distribution of  $CO_2$  relative to a uniform spatial distribution of  $CO_2$  through  $CO_2$ -radiative forcing for the  $j$ th region at the  $t$ th time (units:  $g\ C\ yr^{-1}$ ) and  $NPP_t$  is the NPP for the  $t$ th time period using forcing by a uniform spatial distribution of  $CO_2$  for the whole terrestrial ecosystem.  $C_j$  is the contribution of a non-uniform spatial distribution  $CO_2$  through  $CO_2$ -radiative forcing for the  $j$ th region relative to the global NPP using forcing by a uniform spatial distribution of  $CO_2$ .

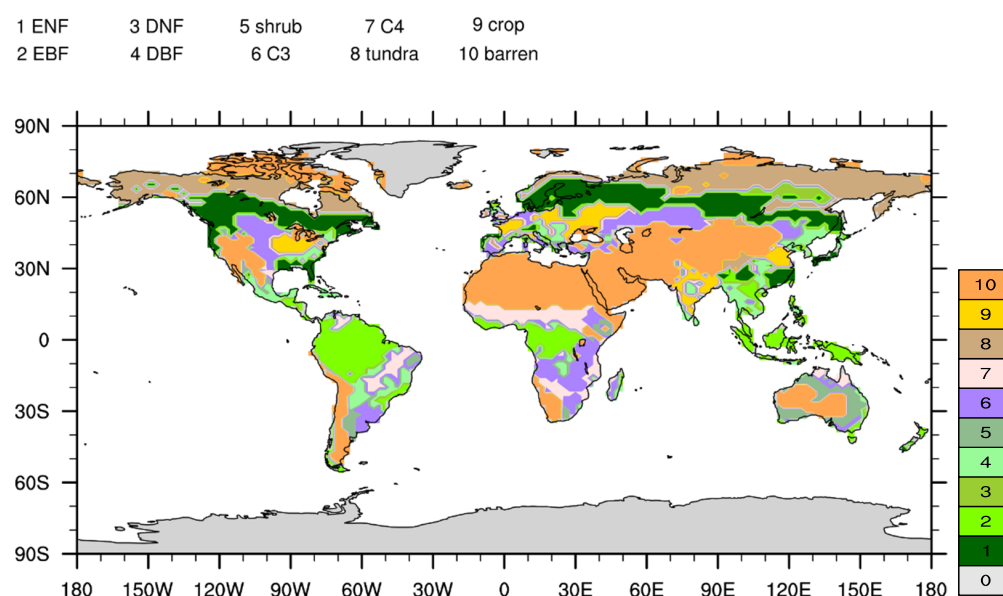


**Figure 1.** Geographical distribution of the 10 plant function types in FGOALS-AVIM. ENF, evergreen needle leaf forest; EBF, evergreen broadleaf forest; DBF, deciduous broadleaf forest.

FGOALS that we used here participated in the CMIP6 and was used as an assessment tool in the 6th Assessment Report of the Intergovernmental Panel on Climate Change. It is a fully coupled earth system model and is composed of four separate models simultaneously simulating the Earth's atmosphere (SAMIL2), oceans (LICOM2), land surface (AVIM) and sea ice (CSIM). FGOALS includes one central coupler component (CPL6). It has an interactive carbon cycle model in the land component and an ecosystem-biogeochemical module in the ocean component. The simulated atmospheric  $CO_2$  concentrations are fully coupled to the land  $CO_2$  fluxes and are used directly to compute radiative forcing. The release of methane from the melting of permafrost potentially has a huge impact on warming, but FGOALS-AVIM currently has only very simple carbon permafrost models and no release of marine methane is included.

We used FGOALS-AVIM at a resolution of  $(2.81^\circ \times 1.66^\circ)$  [22]. This version of FGOALS has previously been used to assess the effects of  $CO_2$ -radiative forcing on the total cloud fraction, temperature and water vapor under different abruptly quadrupling  $CO_2$  concentrations [23]. Evaluation of the mean summer evapotranspiration and mean annual runoff in the Lake Baikal basin [24], and major global biogeochemical fluxes and pool sizes of carbon [25–28].

Time series of the atmospheric  $CO_2$  concentrations (i.e., fossil fuel burning, cement manufacturing and gas flaring in oilfields) from CMIP6 are available from 1850 to 2014 at a monthly resolution. The atmospheric  $CO_2$  variable from CMIP6 only considers spatial variations in terms of latitude rather than longitude. We therefore used the Open-Data Inventory for Anthropogenic Carbon dioxide (ODIAC) [29] at a resolution of  $(1^\circ \times 1^\circ)$  to establish a quantitative relationship between the carbon emissions in each pixel and the latitudinally averaged carbon emissions to fully reflect the spatial heterogeneity of atmospheric  $CO_2$  and to describe the impact of anthropogenic carbon emissions on its spatial distribution in the atmosphere. We assumed that this quantitative relationship is

also applicable to the relationship between the atmospheric CO<sub>2</sub> variable of each pixel and the latitudinally averaged atmospheric CO<sub>2</sub> from CMIP6. The CO<sub>2</sub> variable was produced by fully considering the spatial heterogeneity, which reflected the effect of anthropogenic carbon emissions. The CO<sub>2</sub> variables for 1850–2005 were generated by re-gridding from a spatial resolution of (1° × 1°) to (2.81° × 1.66°). The CO<sub>2</sub> variable was then used as input data for our model.

To quantify the effects of a non-uniform spatial distribution of CO<sub>2</sub> on the carbon flux through CO<sub>2</sub>-radiative forcing, we carried out two different simulations using FGOALS-AVIM with one of the two different components used to estimate NPP. We ran each experiment for a simulated 156 years from 1850 to 2005 (Table 1). Simulation A1 includes the non-uniform space–time-varying atmospheric concentrations of CO<sub>2</sub> based on the active atmosphere–land–ocean–sea ice components. Simulation A2 fixes only one atmospheric CO<sub>2</sub> level at the global scale with only the time-varying atmospheric concentrations of CO<sub>2</sub> without the spatial variations described by [30] and fully considers the interactions of the atmosphere–land–ocean–sea ice components. Simulation B1 uses the non-uniform time–space-varying atmospheric concentrations of CO<sub>2</sub> and the coupled atmosphere–land interactions without ocean and sea ice dynamics. Simulation B2 uses the uniform time-varying atmospheric concentrations of CO<sub>2</sub> and the coupled atmosphere–land interactions without ocean and sea ice dynamics.

**Table 1.** Forcing data for simulations.

Simulation	CO <sub>2</sub> Forcing	Component
A1	Spatial and temporal variations	Fully coupled atmosphere–land–ocean–sea ice
B1	Only temporal variations	Fully coupled atmosphere–land–ocean–sea ice
A2	Spatial and temporal variations	Only atmosphere–land coupling
B2	Only temporal variations	Only atmosphere–land coupling

The difference in the land NPP between simulations A1 and A2 or simulations B1 and B2 represents the effect of the non-uniform spatial distribution of atmospheric concentrations of CO<sub>2</sub>. It is well known that physiological forcing is a robust driver influencing terrestrial plants and the accumulation of carbon on land [17,31], but we did not consider physiological forcing in the land component, in which atmospheric concentrations of CO<sub>2</sub> were fixed at the current level of ~355 ppmv.

Simulated NPP from TRENDY used in this study can be freely downloaded from TRENDY | Dynamic Global Vegetation Model Projects (ceh.ac.uk) (see Table 2). The selected models mainly include CLM4C, CLM4CN, LPJ, LPJGUESS, OCN, SDGVM, TRIFFID and CABLE. The natural response of NPP across the terrestrial ecosystem is one of our focuses. Thus, S2 experiment from TRENDY was chosen, which did not include the impact of land use. For more detailed information about TRENDY simulation protocol could be seen in [32,33]. Previous studies have proved that results of TRENDY perform well and are also widely used to estimate the global carbon budget [6]. Compared with the observed data, TRENDY reproduced variations in carbon fluxes of the terrestrial ecosystem to a certain extent [34,35].

**Table 2.** Datasets used in this study.

Variable	Project	Period	Website	Ref.
NPP	TRENDY	1956–2005	TRENDY   Dynamic Global Vegetation Model Projects (ceh.ac.uk)	[32]
CO <sub>2</sub> emission	ODIAC	1980–2014	<a href="https://db.cger.nies.go.jp/dataset/ODIAC/DL_odiad_v1.7.html">https://db.cger.nies.go.jp/dataset/ODIAC/DL_odiad_v1.7.html</a> (accessed on 19 August 2019).	[29]



### 3. Results

Under historical conditions from 1956 to 2005, NPP from simulations A1, A2, B1, and B2 was estimated. The spatial distribution of PFT is shown in Figure 1. In the following results, at the PFT level, the changes in NPP caused by the non-uniform distribution of CO<sub>2</sub> would be given.

#### 3.1. Estimates of CO<sub>2</sub> Concentrations and NPP

There was a large spatial heterogeneity in atmospheric concentrations of CO<sub>2</sub> between the northern and southern hemispheres in the time period 1956–2005. The non-uniform spatial distribution of CO<sub>2</sub> was lower in Australia, most of Africa and southern South America, but higher in southern Europe, the eastern USA and southeast Asia. During the same time period, simulations A1 and B1 were driven by the same CO<sub>2</sub>-radiative forcing and simulations A2 and B2 were enforced by the same CO<sub>2</sub> data. The spatial variations in CO<sub>2</sub> ranged between 339 and 351 ppmv (Figure 2a). Greater differences between simulations A1 and A2 or B1 and B2 were mainly located in southern Europe, the eastern USA and southeast Asia (Figure 2b).

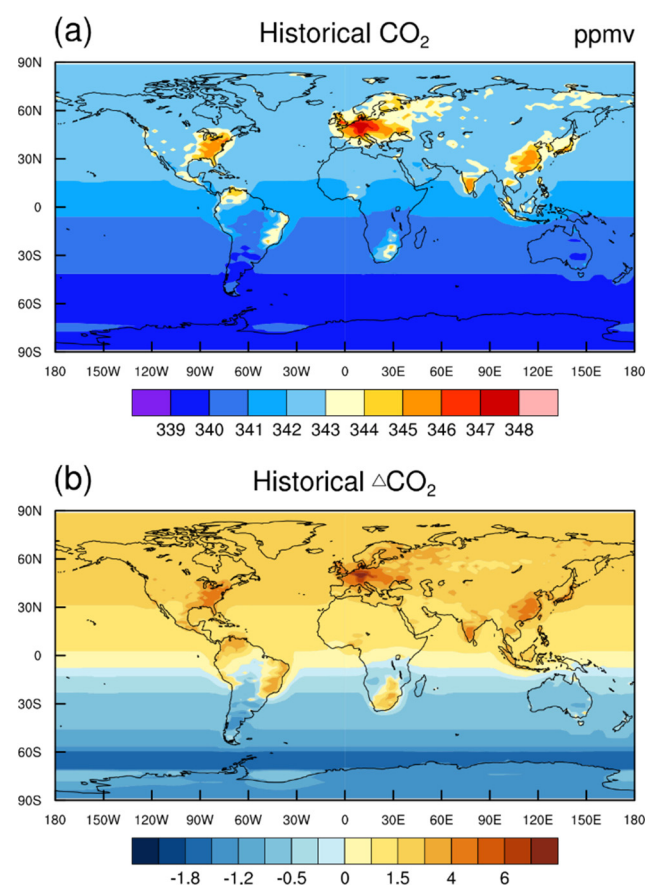


**Figure 2.** (a) Spatial variation in the mean annual atmospheric CO<sub>2</sub> concentrations during the time period 1956–2005 estimated by FGOALS-AVIM. (b) Mean annual changes in CO<sub>2</sub> concentrations during the time period 1956–2005 estimated by simulation A1 relative to A2 or simulation B1 relative to B2.

The NPP was estimated for simulations A1, A2, B1 and B2 during the time period 2000–2005 under current conditions. This period was chosen so that our results were comparable with NPP data from the TRENDY datasets. The TRENDY dataset consists of an ensemble of seven process-based terrestrial ecosystem model simulations [36]. We selected experiment S2 without land use changes and fires and including CLM4C, CLM4CN, LPJ, LPJ-GUESS, OCN, SDGVM and TRIFFID [37] from 1901 to 2010.

Our estimated land NPP for the four simulations of  $51.39\text{--}56.47\text{ Pg C yr}^{-1}$  was lower than the estimates of about  $70\text{ Pg C yr}^{-1}$  of [38], but higher than the  $41\text{ Pg C yr}^{-1}$  estimated by [39]. The estimated NPPs of the four simulations were closer to the observed estimate of about  $56.02\text{ Pg C yr}^{-1}$  of [40]. Globally, the mean annual NPP in the historical period from CMIP5 was about  $62.6\text{ Pg C yr}^{-1}$  [41], whereas it was  $55.53 \pm 1.69\text{ Pg C yr}^{-1}$  from the TRENDY dataset. The mean annual NPP in the historical period simulated by FGOALS-AVIM was  $53.80 \pm 2.54$ ,  $53.75 \pm 2.95$ ,  $58.75 \pm 1.46$  and  $59.36 \pm 2.73\text{ Pg C yr}^{-1}$  from simulations A1, A2, B1 and B2, respectively (Figure 3).

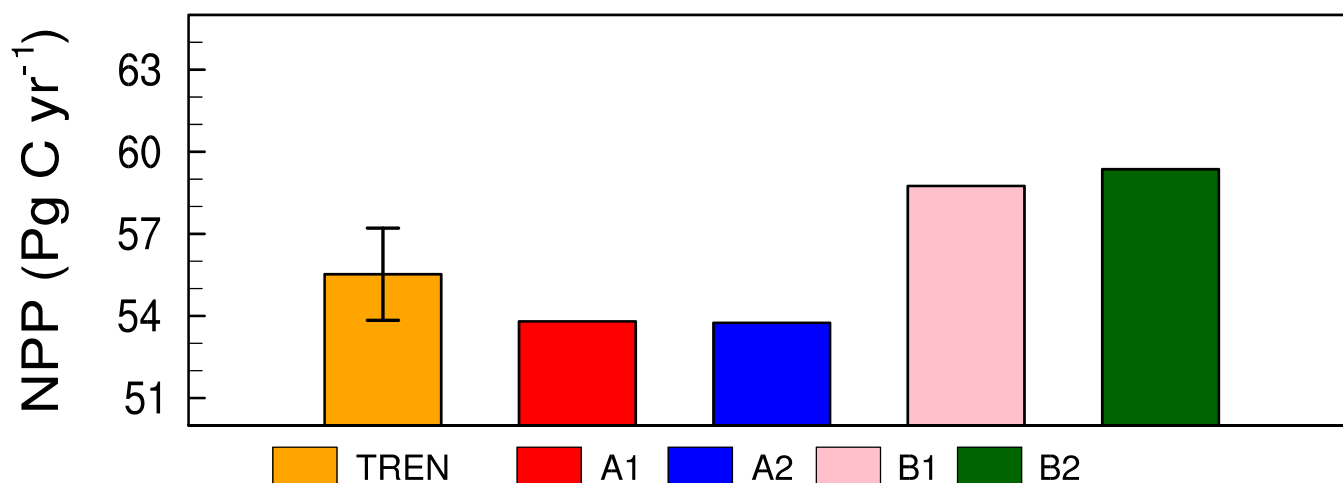


**Figure 3.** From 1956 to 2005, comparison of different estimates of net primary production based on the TRENDY ensemble (TREN, orange bar) taking into consideration the spatial heterogeneity of atmospheric CO<sub>2</sub> concentrations in the fully coupled atmosphere–land–ocean–sea ice components of FGOALS-AVIM (A1, red bar), the fully coupled atmosphere–land–ocean–sea ice components of FGOALS-AVIM without the spatial heterogeneity of atmospheric CO<sub>2</sub> concentrations (A2, blue bar), the spatial heterogeneity of atmospheric CO<sub>2</sub> concentrations with only atmosphere–land coupling in FGOALS-AVIM (B1, pink bar) and only atmosphere–land coupling without the spatial heterogeneity of atmospheric CO<sub>2</sub> concentrations (B2, green bar).

### 3.2. Estimates of Climatic Variables under Present Conditions

Over the simulation period 1956–2005, the non-uniform spatial distribution of CO<sub>2</sub> through CO<sub>2</sub>-radiative forcing resulted in a global increase in low cloudiness of about  $0.002\% \pm 0.005\%$  (Figure 4a), a net solar flux of  $0.52 \pm 0.55\text{ W m}^{-2}$  including the atmosphere–land–ocean–sea ice dynamics (Figure 4e) and a terrestrial latent heat flux of  $0.36 \pm 0.97\text{ W m}^{-2}$  at the global scale (Figure 4c). At the global scale, the climate variables varied considerably among the different components in response to the non-uniform spatial distribution of CO<sub>2</sub> through CO<sub>2</sub>-radiative forcing. During the time period 1956–2005, the non-uniform spatial distribution of CO<sub>2</sub> through CO<sub>2</sub>-radiative forcing based on only atmosphere and land interactions caused an increase in the net solar flux of about  $0.45 \pm 0.31\text{ W m}^{-2}$  and a decrease in global low cloudiness of  $0.001\% \pm 0.003\%$ , especially over the ocean (Figure 4b; Table 3). By contrast, the simulated global latent heat flux based on atmosphere and land interactions decreased by about  $-0.64 \pm 0.93\text{ W m}^{-2}$  (Figure 4d).

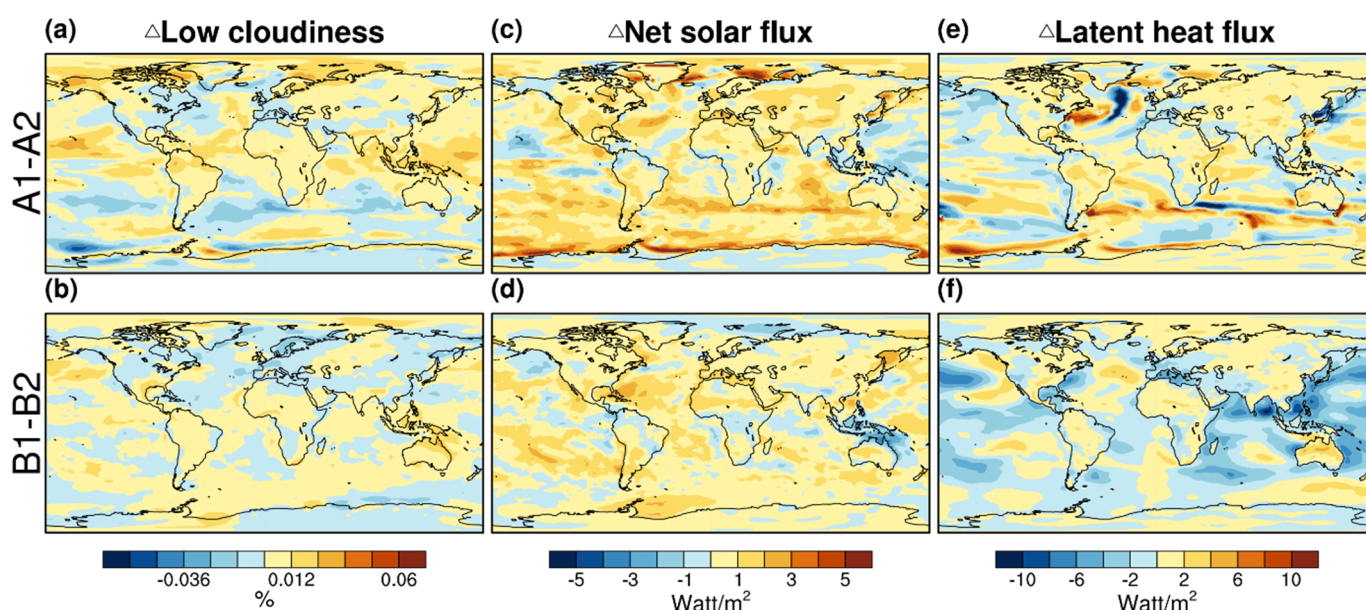


**Figure 4.** (a,b) Response of the mean annual low cloudiness to the spatial heterogeneity of CO<sub>2</sub> concentrations over the time period 1956–2005 estimated from simulation A1 or B1 relative to A2 or B2, respectively. (c,d) Spatial changes in the mean annual net solar flux at the Earth’s surface estimated from simulation A1 or B1 relative to A2 or B2, respectively. (e,f) Spatial changes in the mean annual latent heat flux estimated from simulation A1 or B1 relative to A2 or B2, respectively.

**Table 3.** Response of variables to CO<sub>2</sub>-radiative forcing as a result of the non-uniform spatial distribution of CO<sub>2</sub>.

Variable	Range	A1–A2	B1–B2
CO <sub>2</sub>	Global	$-0.0007 \pm 0.0037$	
Precipitation (mm yr <sup>-1</sup> )	Land	$6.77 \pm 21.45$	$-9.26 \pm 14.72$
	Ocean	$5.89 \pm 14.15$	$-9.58 \pm 9.92$
Surface temperature (°C)	Land	$0.57 \pm 0.45$	$0.02 \pm 0.05$
	Ocean	$0.45 \pm 0.38$	$0.07 \pm 0.08$
Latent heat flux (W m <sup>-2</sup> )	Land	$0.59 \pm 1.23$	$-0.64 \pm 0.93$
	Ocean	$0.38 \pm 0.80$	
Sensible heat flux (W m <sup>-2</sup> )	Land	$-0.29 \pm 0.46$	
	Ocean	$-0.20 \pm 0.42$	
Net radiation flux at Earth’s surface (W m <sup>-2</sup> )	Land	$0.79 \pm 0.69$	
	Ocean	$0.59 \pm 0.63$	
Soil evaporation (kg m <sup>-2</sup> yr <sup>-1</sup> )	Land	$3.99 \pm 7.52$	
Vegetation evaporation (kg m <sup>-2</sup> yr <sup>-1</sup> )	Land	$0.43 \pm 4.90$	
Soil transpiration (kg m <sup>-2</sup> yr <sup>-1</sup> )	Land	$1.91 \pm 5.70$	
Surface runoff	Land	$3.00 \pm 6.18$	
Soil moisture (kg m <sup>-2</sup> )	Land	$0.03 \pm 0.04$	

To further analyze the causes of the differences in the estimated NPP resulting from the non-uniform spatial distribution of CO<sub>2</sub> through CO<sub>2</sub>-radiative forcing, we estimated the changes in the vital variables (e.g., surface temperature, precipitation, evapotranspiration and soil moisture in the different components) for the historical time period 1956–2005. Non-uniform CO<sub>2</sub> from simulations fully coupled atmosphere–land–ocean–sea ice components caused an increase in surface temperature ranging from  $0.57 \pm 0.45$  °C in the terrestrial ecosystem, where it from simulations only coupled atmosphere and land without active ocean and sea ice components led to less increased surface temperature of  $0.02 \pm 0.05$  °C. The changes in the surface temperature at the regional level correspond well to the changes in the non-uniform spatial distribution of CO<sub>2</sub> considering only the atmosphere–land interactions (Figure 5b). The responses of the surface temperature in tropical regions to the non-uniform spatial distribution of CO<sub>2</sub> through CO<sub>2</sub>-radiative forcing based on the fully

coupled atmosphere–land–ocean–sea ice components were up to  $>0.2$  °C, especially in the Amazon basin, central Africa and tropical Asia. By contrast, the simulations with only the atmosphere–land interactions simulated a small increase or even decrease in these regions.

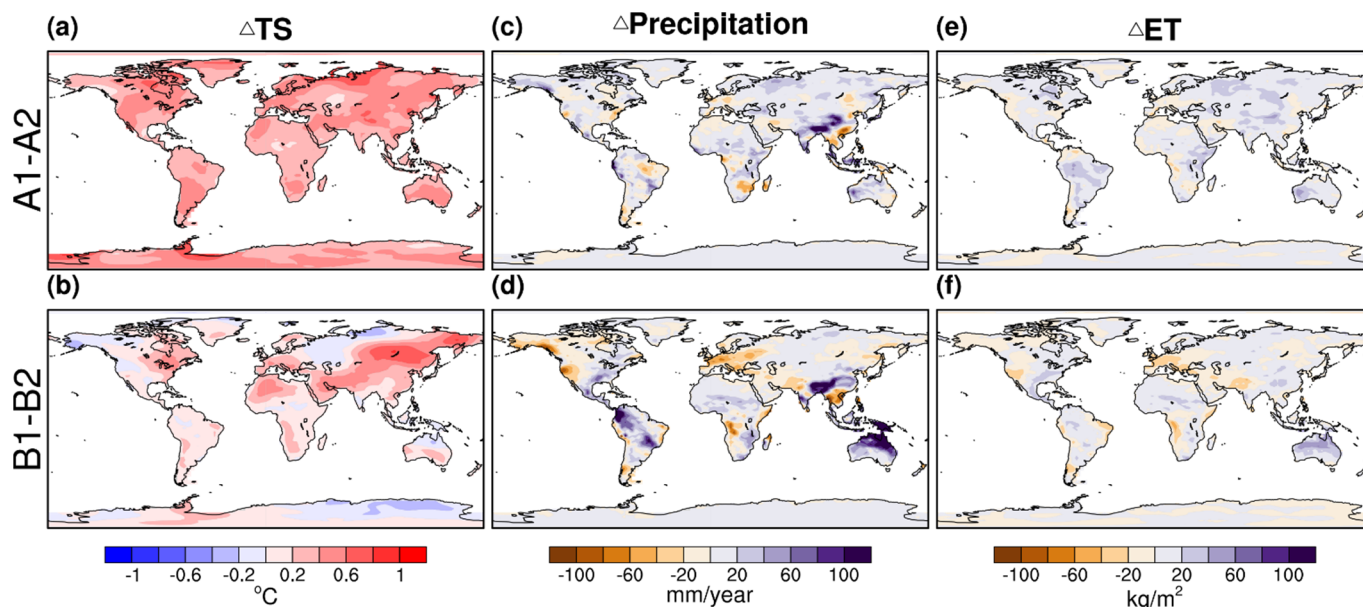


**Figure 5.** (a,b) Response of the mean annual surface temperature to the spatial heterogeneity of CO<sub>2</sub> concentrations over the time period 1956–2005 estimated from simulation A1 or B1 relative to A2 or B2, respectively. (c,d) Spatial changes in precipitation estimated from simulation A1 or B1 relative to A2 or B2, respectively. (e,f) Spatial changes in the mean evapotranspiration estimated from simulation A1 or B1 relative to A2 or B2, respectively.

In the time period 1956–2005, precipitation over the land surface increased in most of the northern hemisphere, but not in southern Europe, the eastern USA and southeast Asia. This was a response to the non-uniform spatial distribution of CO<sub>2</sub> through CO<sub>2</sub>-radiative forcing (Figure 5c) compared with the uniform spatial distribution of CO<sub>2</sub> in the same period. The simulated increase in precipitation influenced by non-uniform spatial distribution of CO<sub>2</sub> considering the full atmosphere–land–ocean–sea ice interactions was much greater than that which considered only atmosphere–land interactions, apart from in the Amazon basin and tropical Asia. This was a result of the larger increase in the net radiation flux from surface warming and latent heat flux over land, especially in the northern hemisphere.

Correspondingly, the responses of the simulated change in evapotranspiration by the two differently coupled components differed considerably in both the direction and magnitude of change for most terrestrial ecosystems (Figure 5d,e). The two different components predicted an increase in evapotranspiration affected by the non-uniform spatial distribution of CO<sub>2</sub> through CO<sub>2</sub>-radiative forcing relative to the uniform spatial distribution of CO<sub>2</sub> for most land surfaces. The simulated response of evapotranspiration to changes in the non-uniform spatial distribution of CO<sub>2</sub> differed at the regional scale. For example, evapotranspiration north of 50° N in the northern hemisphere was predicted to increase as a response to the uniform spatial distribution of CO<sub>2</sub> through CO<sub>2</sub>-radiative forcing based on the fully coupled atmosphere–land–ocean–sea ice model, but to decrease in southern Europe, the eastern USA and southeast Asia. By contrast, evapotranspiration influenced by the non-uniform spatial distribution of CO<sub>2</sub> considering only the atmosphere–land interactions showed a much greater increase than the fully coupled atmosphere–land–ocean–sea ice interactions at low latitudes and in the eastern USA.



### 3.3. Responses of NPP to Spatial Varying of CO<sub>2</sub> Concentrations through Radiative Forcing

To quantify the impact of the non-uniform spatial distribution of CO<sub>2</sub> on NPP, we simulated the NPP for the time period 1956–2005 with or without the uniform spatial distribution of CO<sub>2</sub> after 1850. Specifically, we ran FGOALS-AVIM with CO<sub>2</sub> held at the same value at the global level for each land grid point in simulation A2 or B2 and compared the results with the non-uniform spatial distribution of CO<sub>2</sub> for each land grid point in simulation A1 or B1 for the time period 1956–2005.

We estimated that the decrease in NPP caused by the non-uniform spatial distribution of CO<sub>2</sub> through CO<sub>2</sub>-radiative forcing during the time period 1956–2005 was  $-3.39 \pm 12.33 \text{ g C m}^{-2} \text{ yr}^{-1}$  or about  $-0.5 \pm 1.88 \text{ Pg C yr}^{-1}$  for the fully coupled atmosphere–land–ocean–sea ice components (simulation A1 minus A2). The increase was about  $0.88 \pm 8.86 \text{ g C m}^{-2} \text{ yr}^{-1}$  or  $0.1 \pm 1.35 \text{ Pg C yr}^{-1}$  when considering only atmosphere–land interactions (Figure 6a,b).

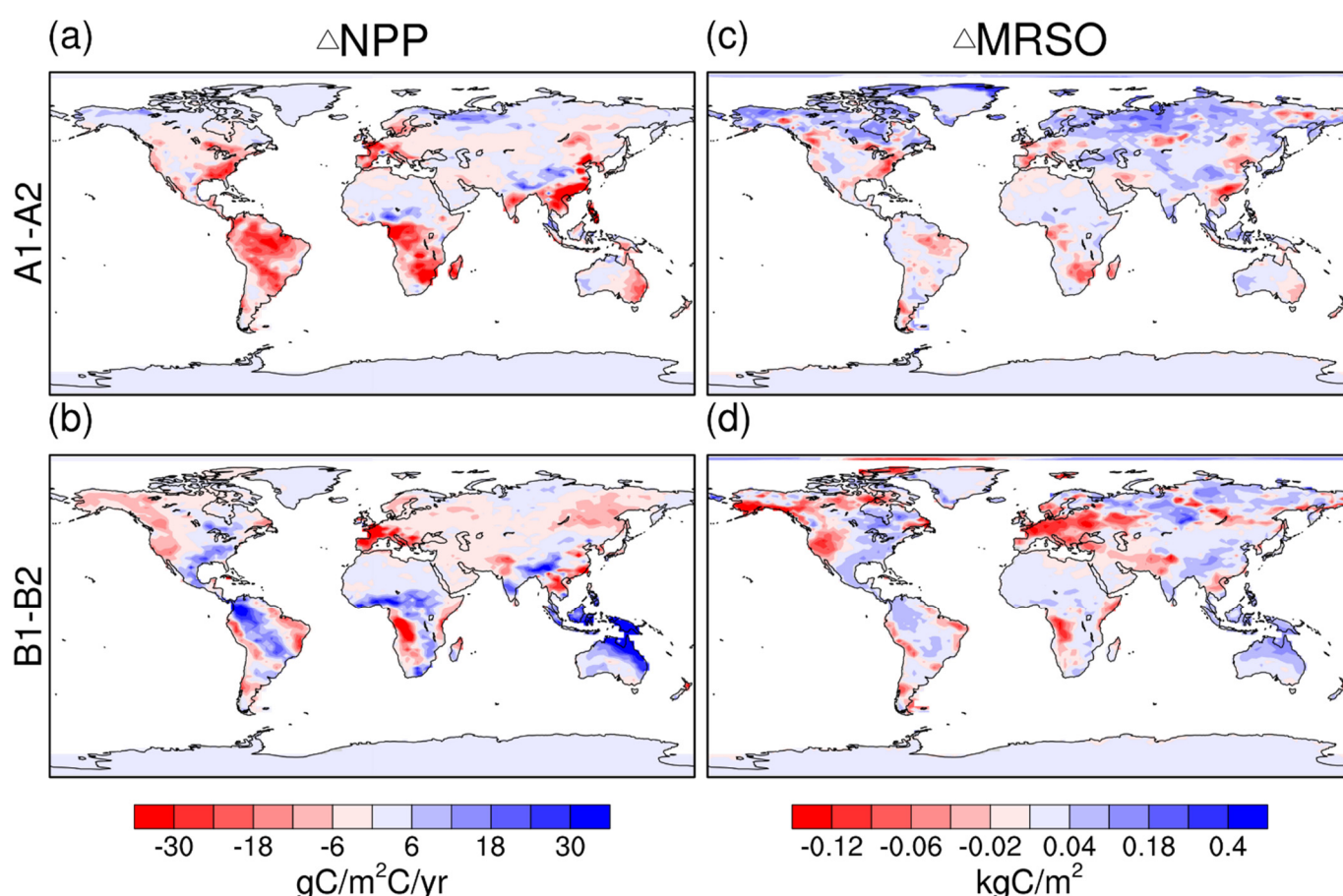


**Figure 6.** (a,b) Response of the mean net primary production to the spatial heterogeneity of CO<sub>2</sub> concentrations over the time period 1956–2005 estimated from simulation A1 or B1 relative to A2 or B2, respectively. (c,d) Spatial changes in soil moisture estimated from simulation A1 minus A2 or B1 minus B2, respectively.

The fully coupled atmosphere–land–ocean–sea ice components estimated a decrease in NPP caused by the non-uniform spatial distribution of CO<sub>2</sub> through CO<sub>2</sub>-radiative forcing for terrestrial ecosystems (Figure 6a), whereas the coupled active atmosphere–land components predicted an increase (Figure 6b). The mechanism contributing to the estimated change in NPP was similar between the two simulations. With the simulated decrease in soil moisture (Figure 6c), the model based on the fully coupled atmosphere–land–ocean–sea ice components estimated a decrease in NPP for southern Europe, the eastern USA, southeast Asia, the Amazon basin and central Africa (Figure 6a). However, the simulation considering only the atmosphere–land interaction estimated an increase in soil



moisture (Figure 4d) for the eastern USA, the Amazon basin and central Africa (Figure 6d). The estimated increase in NPP for these regions using only the active atmosphere–land components was attributed to the relatively higher increase in NPP (Figure 6b).

We used the present vegetation cover for the period of the 1990s based on the plant functional types (PFTs) of the International Geosphere Biosphere Program (IGBP) data [42]. At the PFT-level, the NPP simulated by simulations A due to spatial varying in CO<sub>2</sub> concentrations were reduced for EBF, DBF, C4 and crop, but increased for tundra. The variations in NPP simulated from simulations A and B were feeble for ENF. Globally, the changes of annual NPP from 1956 to 2005 resulting from varying in CO<sub>2</sub> concentrations was  $\sim -0.5$  Pg C yr<sup>-1</sup> from simulations A or estimates of  $\sim 0.1$  Pg C yr<sup>-1</sup> from simulations B (Supplementary Materials Figure S1).

The non-uniformity of CO<sub>2</sub> leads to substantial changes in surface temperature and water fluxes, and the changes caused by non-uniformity of CO<sub>2</sub> in NPP depend on changes in surface temperature and soil moisture, rather than the impact of CO<sub>2</sub>, which may lead to changes in the spatial distribution of NPP (Figure 7). Figure 7b,e show how much change in NPP is locally related to changes in surface temperature, especially in the tropics and the Southern Hemisphere. Obviously, these two variables are significantly correlated, which indicates that changes in surface temperature can explain the changes in NPP in these regions. For example, considering that the fully coupled land-atmosphere-ocean-ice interaction, rising surface temperature leads to negative changes of NPP in tropics due to non-uniform CO<sub>2</sub>. On the contrary, in most terrestrial ecosystems, there is a significantly positive correlation between soil moisture and local NPP ( $p < 0.05$ ) (Figure 7c,f). Therefore, our results indicate that the competition between the impacts of surface temperature and soil moisture on NPP is one of the mechanisms leading to changes in NPP in the tropics.

Although the absolute change in CO<sub>2</sub> at the global scale was estimated to be only about 0.3%, the model based on coupled components A1 minus A2 or B1 minus B2 estimated an additional change in NPP caused by the non-uniform spatial distribution of CO<sub>2</sub> by 14.26% or 11.51% during the time period 1956–2005 (Figure 8). This reflects that the impact of CO<sub>2</sub> heterogeneity on carbon cycle was amplified by the climate effect. In addition, the difference between the two different coupled components probably reflects the contribution of the ocean and sea ice to the climate system. With global warming caused by the non-uniform spatial distribution of CO<sub>2</sub> through CO<sub>2</sub>-radiative forcing, the model based on the fully coupled components A1 minus A2 estimated absolute variations in NPP caused by the non-uniform spatial distribution of CO<sub>2</sub> relative to the global NPP driven by a uniform spatial distribution of CO<sub>2</sub> ranging from 0.97 to 1.53% for C3 and from 2.92 to 4.03% for crops. The simulation with only atmosphere–land interactions ranged from 1.76 to 2.23% for C3 and from 2.56 to 3.32% for crops. For different PFTs (e.g., crops), the absolute changes in CO<sub>2</sub> from 0.05 to 0.10% were estimated to be higher than those for other PFTs. The impact of the non-uniform spatial distribution of CO<sub>2</sub> was largest for deciduous broadleaf forest, for which simulation A1 minus A2 estimated higher absolute changes in NPP from 2.53 to 4.65% for evergreen broadleaf forest due to the non-uniform spatial distribution of CO<sub>2</sub>, compared with simulation B1 minus B2 from 1.93 to 3.05%. For crops, both simulations A1 minus A2 and B1 minus B2 estimated high absolute changes ranging from 2.56 to 3.32%.

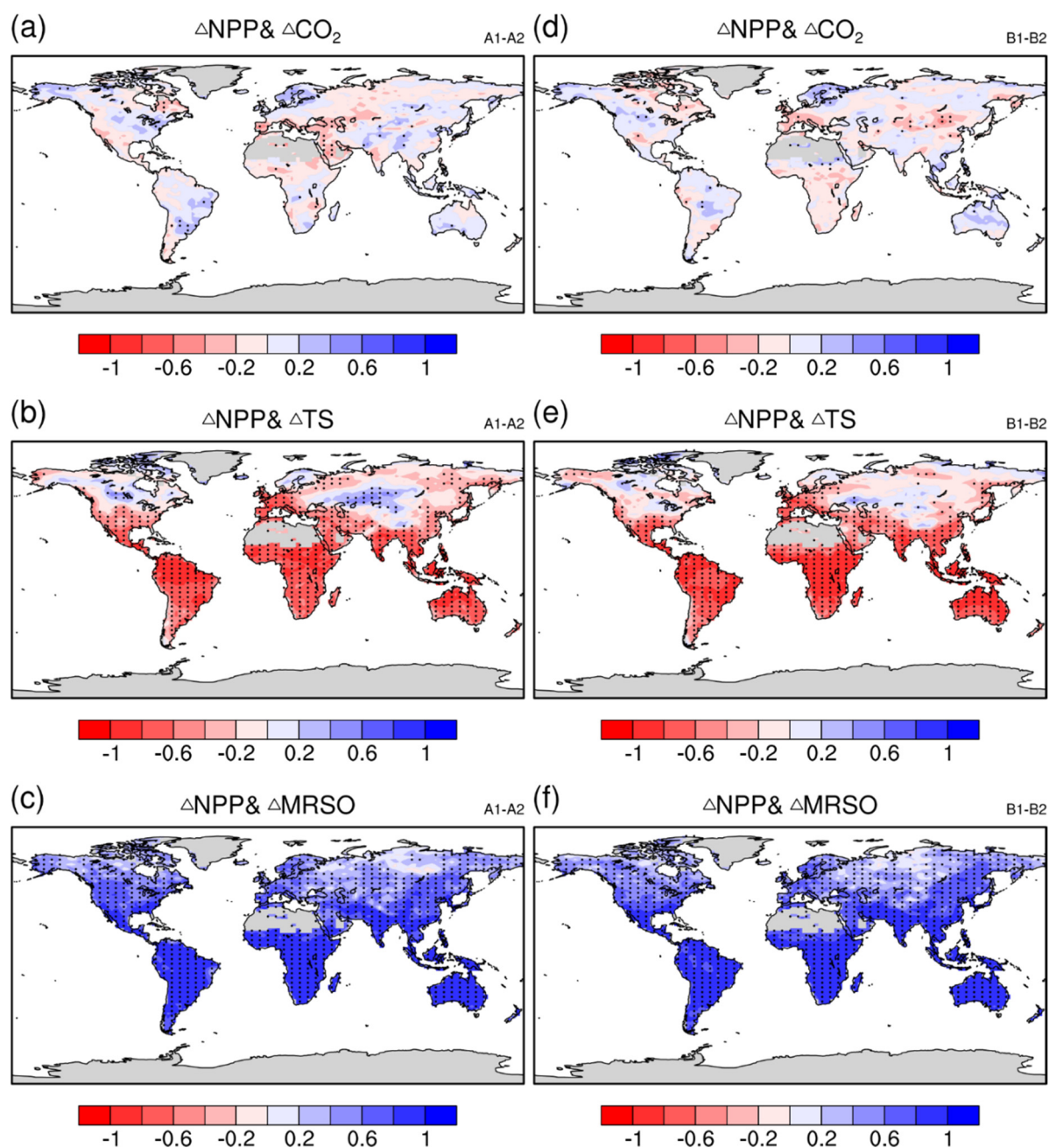


**Figure 7.** (a–c) Linear correlation coefficients of changes in  $\text{CO}_2$  concentrations, the surface temperature (TS), soil moisture (MRSO) to NPP over the time period 1956–2005 estimated from simulation A1 relative to A2, respectively. (d–f) Linear correlation coefficients of changes in  $\text{CO}_2$  concentrations, the surface temperature (TS), soil moisture (MRSO) to NPP over the time period 1956–2005 estimated from simulation B1 relative to B2, respectively. Dotted areas are areas with statistically significant changes at the 5% level using Student's *t*-test.

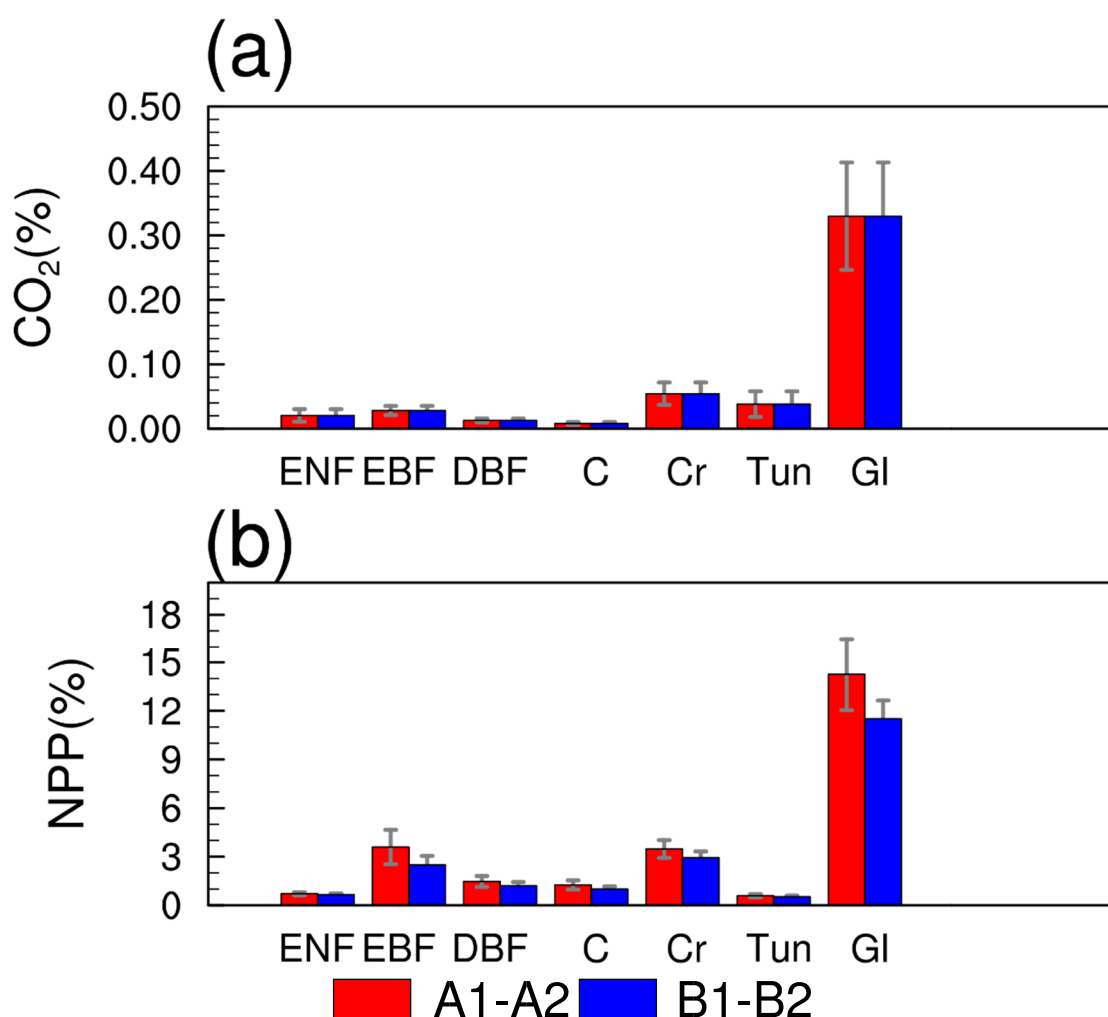


**Figure 8.** Changes in (a) CO<sub>2</sub> concentrations (units: %) and (b) net primary production (NPP) (units: %) over the time period 1956–2005 from simulation A1 or B1 relative to A2 or B2 as estimated using FGOALS-AVIM over different plant function types. ENF, evergreen needle leaf forest; EBF, evergreen broadleaf forest; DBF, deciduous broadleaf forest; C, C<sub>4</sub>; Cr, crop; Gl, global. Error bar are  $\pm$ SD calculated from model simulations over the same time period.

#### 4. Discussion

At present, few studies have considered effect of radiative forcing of spatial varying of CO<sub>2</sub> concentrations in the atmosphere on NPP. Our results showed that the non-uniform spatial distribution of CO<sub>2</sub> through CO<sub>2</sub>-radiative forcing has important implications for carbon fluxes. We estimated that the non-uniform spatial distribution of CO<sub>2</sub> contributed to a decrease in NPP, although most other studies have not considered this. The CMIP5 provides an ensemble mean annual NPP of 62.6 Pg C yr<sup>−1</sup> over the time period 1995–2004 [41]. However, this analysis did not consider the feedbacks from the non-uniform spatial distribution of CO<sub>2</sub> to the Earth's climate system. Our analysis showed an effect of the non-uniform spatial distribution of CO<sub>2</sub> on NPP without considering land use of up to  $14.26 \pm 2.22\%$  of the NPP simulated by a fully coupled model. This highlights the tremendous leverage of a non-uniform spatial distribution of CO<sub>2</sub> on the global carbon cycle and we recommend a more substantial focus on understanding this process in the biosphere through the influence of the climate system based on coupled models that include dynamical sea ice and ocean components.

In the past 30 years, there has been an increase in NPP at the global scale, which is likely driven by CO<sub>2</sub> fertilization [34,35]. However, the increase in CO<sub>2</sub> radiative forcing limits this positive effect [1]. The exact impact of spatial varying in CO<sub>2</sub> concentration on the carbon cycle through radiative forcing is not yet fully understood. Our study illuminates that from 1956 to 2005, the spatial varying in the CO<sub>2</sub> concentration resulted in a reduction of NPP, which mainly occurred in the tropics and the middle-latitudes of the Northern Hemisphere. Nevertheless, as shown in Figure 7, a relationship between variations in CO<sub>2</sub> concentration and NPP could not pass a significant level. It might result due to not considering the impact of CO<sub>2</sub> fertilization. On the contrary, spatial varying in CO<sub>2</sub> concentration through the radiation effect influences temperature, precipitation and soil moisture, which ultimately affects NPP. The northern hemisphere accounts for nearly 68% of the global area, which has a higher CO<sub>2</sub> concentration than the globally averaged level. Higher temperature has a negative impact on NPP in tropics and mid-latitudes of the Northern Hemisphere [33,38,43,44]. In addition, considering ocean feedback, an increase in temperature could reduce NPP in these regions. Conversely, when the ocean feedback is shielded, increases in temperature is slight in tropics. At the same time, in this condition, the increase in the soil moisture would offset the negative impact of warming in tropics.

To estimate the contribution of the ocean and sea ice influenced by the spatial varying of CO<sub>2</sub> concentrations through CO<sub>2</sub>-radiative forcing to the terrestrial NPP, we carried out simulations B1 and B2, in which the effect of CO<sub>2</sub>-radiative forcing was assessed using fixed the sea surface temperature (SST) in 1980. The additional increase in SST was estimated to be  $0.45 \pm 0.38$  °C using the fully coupled model, compared with  $0.07 \pm 0.08$  °C based on only the coupled active atmosphere–land components. This can be understood by the positive feedback from a greater increase in the SST (Figure 9a) to surface temperature from simulations A1 minus A2 relative to from simulations B1 minus B2 without varying SST. The response of NPP in low-latitudes of terrestrial ecosystem to changes in surface temperature might be asymmetric. This may also lead to asymmetric NPP changes related to SST changes. For example, in some tropical terrestrial regions, increased SST has a negative impact on NPP under warmer changes [45]. Therefore, more detailed quantification is needed to understand the asymmetric response of NPP to SST changes.

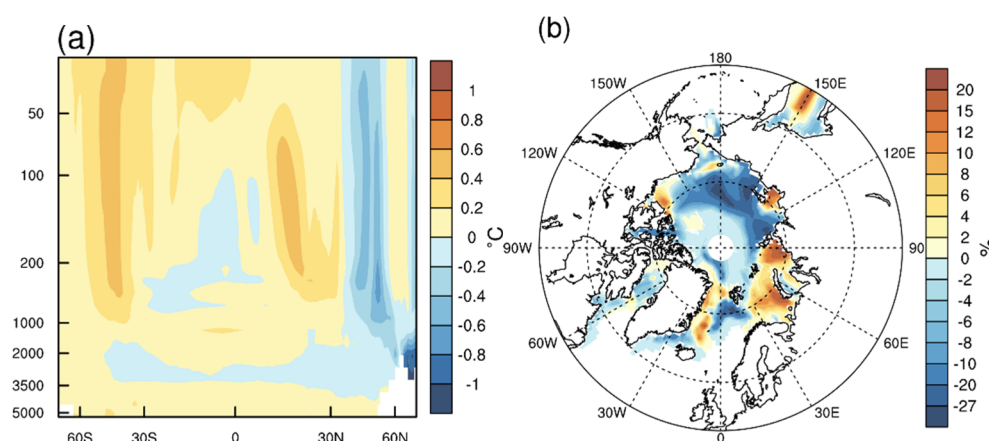


**Figure 9.** Modeled patterns for zonal changes in (a) ocean temperature with depth (units: °C) and (b) the fraction of ice area (units: %) in the time period 1956–2005 in FGOALS-AVIM simulation A1 relative to A2.

The spatial response of soil moisture differed widely, although the SST had a key influence soil moisture [46]. Under warmer conditions, a non-uniform spatial distribution of CO<sub>2</sub> decreased soil moisture across the eastern USA, southern Europe and southeast Asia in the fully coupled model. This is consistent with previous research [47], which showed that an increased SST in the tropics would increase the depletion of soil moisture in the eastern USA, southern Europe, southeast Asia and the tropics.

At high latitudes (e.g., the Arctic), the decrease in the area of ice as a result of the non-uniform spatial distribution of CO<sub>2</sub> through CO<sub>2</sub>-radiative forcing is >2% (Figure 9b). An additional increase in precipitation has been shown in most of this region. This change can be explained by emergent positive feedbacks between the increasing area of melted ice and the increased water vapor at high latitudes in the fully coupled model. Recent studies have found that a decrease in Arctic sea ice has an important role in the Earth's climate and ecosystems [48]. Specifically, stronger warming results in an increased loss of sea ice, which, in turn, simulates more melting through a reduced albedo [48]. Ice-loss feedback could amplify changes in the Earth's climate at high latitudes [48,49]. We estimated larger increases in surface temperature and precipitation for tundra regions using the fully coupled model including sea ice dynamics than the model without sea ice dynamics. There is a positive feedback from an increase in melted sea ice in a warmer and wetter climate, which enhances the NPP by the non-uniform spatial distribution of CO<sub>2</sub> through CO<sub>2</sub>-radiative forcing in the tundra regions.

This finding is consistent with a previous study of CO<sub>2</sub>-radiative forcing and has important implications for our understanding of the changes in carbon flux associated with climate change [50]. Changes in the non-uniform spatial distribution of CO<sub>2</sub> concentrations influenced changes in the heat budget (Figure 4), then continued to regulate the spatial distribution of surface climate variables. Changes in the atmospheric circulation (Figure 10) introduced by the non-uniform spatial distribution of CO<sub>2</sub> also could influence the water balance and, in turn, affect soil moisture. Therefore, the patterns and responses of the water budget at the regional scales triggered by the non-uniform spatial distribution of CO<sub>2</sub> determine the patterns and responses in NPP. In particular, near-global increases in specific humidity do not mean that this increase necessarily results in an increase in precipitation. The simulation using the fully coupled model estimated that weaker westerlies reduced the input of humid air from the Atlantic Ocean to southern Europe, which reduced precipitation and then increased the depletion of soil moisture. The eastward radial circulation in the eastern USA was strengthened. Such a circulation pattern does not favor precipitation. The eastward radial circulation was also enhanced in East Asia and suppressed the monsoon from the Eastern Pacific Ocean, limiting precipitation and inducing droughts.

CO<sub>2</sub>-physiological forcing could also have significant impact on the spatial variation of NPP [51]. However, it was not included in our results, because our main focus is on the impacts of CO<sub>2</sub> radiative forcing on NPP. For terrestrial processes, atmospheric CO<sub>2</sub> was uniformly applied to all PFTs at a fixed level of 355 ppmv. The impact of a spatial variation in CO<sub>2</sub> concentrations was masked in our analysis. Results may be different if we include a variation in the spatiotemporal distribution of atmospheric CO<sub>2</sub> through CO<sub>2</sub>-physiological forcing in the land component. This needs further investigation.



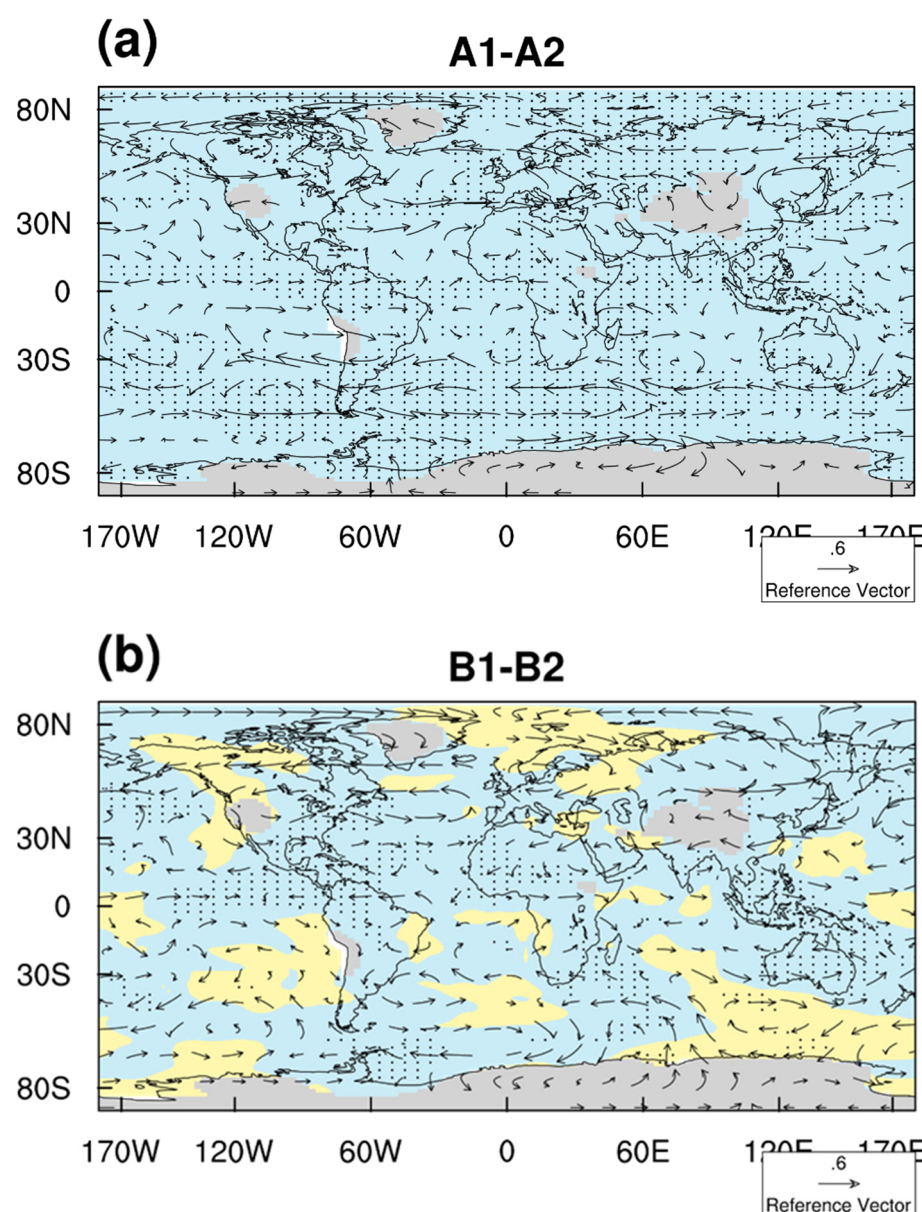


**Figure 10.** (a,b) Spatial changes in the mean specific humidity (units:  $\text{g kg}^{-1}$ ) and 850 hPa winds (vectors;  $\text{m s}^{-1}$ ) over the time period 1956–2005 estimated using FGOALS-AVIM from simulation A1 or B1 relative to A2 or B2, respectively. Dotted areas are areas with statistically significant changes at the 5% level using Student's *t*-test.

## 5. Conclusions

This study investigated the regulations of spatial varying in atmospheric  $\text{CO}_2$  concentration through radiative forcing to annual NPP. The results implied that soil moisture resulting from spatial varying in  $\text{CO}_2$  concentration dominates the changes of annual NPP, and the increased SST substantially reduced NPP in tropics. As a consequence, spatial varying of atmospheric  $\text{CO}_2$  concentration did change the spatial pattern of NPP under the historical conditions from 1956 to 2005. In addition, our results showed the current offline terrestrial models only considering land and atmosphere interactions did not reproduce the feedback of ocean and sea ice to changes in NPP. In general, this study represented the key role of spatial varying in  $\text{CO}_2$  concentration in regulating variations in NPP.

**Supplementary Materials:** The following are available online at <https://www.mdpi.com/article/10.3390/su131910897/s1>, Figure S1: (a) NPP and (b) soil moisture (MRSO) for the globe (GL), evergreen needle leaf forest (ENF); evergreen broadleaf forest (EBF); deciduous broadleaf forest (DBF); crop (C) and tundra (Tun) during the period 1956–2005 caused by the impact of spatial varying of CO<sub>2</sub> concentrations. Horizontal lines in the bars show the maximum and minimum NPP or soil moisture with considering feedbacks of ocean and sea ice (orange) and without considering feedbacks of ocean and sea ice (light blue) from 1956 to 2005.

**Author Contributions:** Conceptualization, methodology, writing—original draft preparation, J.P.; formal analysis, investigation, funding acquisition, L.D.; writing—review and editing, supervision, J.F.; writing—review and editing, supervision, K.Y.; formal analysis, project administration, X.T.; project administration, data curation, F.Y. All authors have read and agreed to the published version of the manuscript.

**Funding:** This work was funded by the National Natural Science Foundation of China (Grant Nos 41630532, 41975112 and 41575093) and the National Key Research and Development Program of China (Grant No. 2016YFA0602501).

**Institutional Review Board Statement:** Not applicable.

**Informed Consent Statement:** Not applicable.

**Data Availability Statement:** Data available on request due to restrictions.

**Conflicts of Interest:** The authors declare no conflict of interest.

## References

1. Friedlingstein, P.; Meinshausen, M.; Arora, V.K.; Jones, C.D.; Anav, A.; Liddicoat, S.K.; Knutti, R. Uncertainties in CMIP5 Climate Projections due to Carbon Cycle Feedbacks. *J. Clim.* **2013**, *27*, 511–526. [\[CrossRef\]](#)
2. Friedlingstein, P. Carbon cycle feedbacks and future climate change. *Philos. Trans. R. Soc. A Math. Phys. Eng. Sci.* **2015**, *373*, 20140421. [\[CrossRef\]](#) [\[PubMed\]](#)
3. Govindasamy, B.; Caldeira, K. Geoengineering Earth's radiation balance to mitigate CO<sub>2</sub>-induced climate change. *Geophys. Res. Lett.* **2000**, *27*, 2141–2144. [\[CrossRef\]](#)
4. Etminan, M.; Myhre, G.; Highwood, E.J.; Shine, K.P. Radiative forcing of carbon dioxide, methane, and nitrous oxide: A significant revision of the methane radiative forcing. *Geophys. Res. Lett.* **2016**, *43*, 12614–12623. [\[CrossRef\]](#)
5. Yuan, W.; Zheng, Y.; Piao, S.; Ciais, P.; Lombardozzi, D.; Wang, Y.; Ryu, Y.; Chen, G.; Dong, W.; Hu, Z.; et al. Increased atmospheric vapor pressure deficit reduces global vegetation growth. *Sci. Adv.* **2019**, *5*, eaax1396. [\[CrossRef\]](#) [\[PubMed\]](#)
6. Schimel, D.; Stephens, B.B.; Fisher, J.B. Effect of increasing CO<sub>2</sub> on the terrestrial carbon cycle. *Proc. Natl. Acad. Sci. USA* **2015**, *112*, 436–441. [\[CrossRef\]](#) [\[PubMed\]](#)
7. Huang, Y.; Xia, Y.; Tan, X. On the pattern of CO<sub>2</sub> radiative forcing and poleward energy transport. *J. Geophys. Res. Atmos.* **2017**, *122*, 10578–10593. [\[CrossRef\]](#)
8. Myhre, G.; Shindell, D.; Bréon, F.-M.; Collins, W.; Fuglestad, J.; Huang, J.; Koch, D.; Lamarque, J.-F.; Lee, D.; Mendoza, B.; et al. Anthropogenic and Natural Radiative Forcing. In *Climate Change 2013: The Physical Science Basis. Contribution of Working Group I to the Fifth Assessment Report of the Intergovernmental Panel on Climate Change*; Cambridge University Press: Cambridge, UK, 2013.
9. Taylor, K.E.; Stouffer, R.J.; Meehl, G.A. An overview of CMIP5 and the Experiment Design. *Bull. Am. Meteorol. Soc.* **2011**, *93*, 485–498. [\[CrossRef\]](#)
10. Nassar, R.; Napier-Linton, L.; Gurney, K.R.; Andres, R.; Oda, T.; Vogel, F.; Deng, F. Improving the temporal and spatial distribution of CO<sub>2</sub> emissions from global fossil fuel emission data sets. *J. Geophys. Res. Atmos.* **2013**, *118*, 917–933. [\[CrossRef\]](#)
11. Falahatkar, S.; Mousavi, S.M.; Farajzadeh, M. Spatial and temporal distribution of carbon dioxide gas using GOSAT data over IRAN. *Environ. Monit. Assess.* **2017**, *189*, 627. [\[CrossRef\]](#)
12. Wang, Y.; Feng, J.; Dan, L.; Lin, S.; Tian, J. The impact of uniform and nonuniform CO<sub>2</sub> concentrations on global climatic change. *Theor. Appl. Climatol.* **2019**, *139*, 45–55. [\[CrossRef\]](#)
13. Friedlingstein, P.; Cox, P.; Betts, R.; Bopp, L.; von Bloh, W.; Brovkin, V.; Cadule, P.; Doney, S.; Eby, M.; Fung, I.; et al. Climate–Carbon Cycle Feedback Analysis: Results from the C4MIP Model Intercomparison. *J. Clim.* **2006**, *19*, 3337–3353. [\[CrossRef\]](#)
14. Ramaswamy, V.; Collins, W.; Haywood, J.; Lean, J.; Mahowald, N.; Myhre, G.; Naik, V.; Shine, K.P.; Soden, B.; Stenchikov, G.; et al. Radiative Forcing of Climate: The Historical Evolution of the Radiative Forcing Concept, the Forcing Agents and their Quantification, and Applications. *AMS Meteorol. Monogr.* **2019**, *59*, 14.1–14.101. [\[CrossRef\]](#)
15. Ballantyne, A.; Smith, W.; Anderegg, W.; Kauppi, P.; Sarmiento, J.; Tans, P.; Shevliakova, E.; Pan, Y.; Poulter, B.; Anav, A.; et al. Accelerating net terrestrial carbon uptake during the warming hiatus due to reduced respiration. *Nat. Clim. Chang.* **2017**, *7*, 148–152. [\[CrossRef\]](#)
16. Cox, P.; Pearson, D.; Booth, B.; Friedlingstein, P.; Huntingford, C.; Jones, C.; Luke, C. Sensitivity of tropical carbon to climate change constrained by carbon dioxide variability. *Nature* **2013**, *494*, 341–344. [\[CrossRef\]](#) [\[PubMed\]](#)

17. Peng, J.; Dan, L.; Dong, W. Are there interactive effects of physiological and radiative forcing produced by increased CO<sub>2</sub> concentration on changes of land hydrological cycle? *Glob. Planet. Chang.* **2014**, *112*, 64–78. [\[CrossRef\]](#)
18. IPCC. Climate Change 2014: Synthesis Report. In *Contribution of Working Groups I, II and III to the Fifth Assessment Report of the Intergovernmental Panel on Climate Change*; IPCC: Geneva, Switzerland, 2014; p. 151.
19. Zhou, T.; Song, F.; Chen, X. Historical evolution of global and regional surface air temperature simulated by FGOALS-s2 and FGOALS-g2: How reliable are the model results? *Adv. Atmos. Sci.* **2013**, *30*, 638–657. [\[CrossRef\]](#)
20. Dan, L.; Cao, F.; Gao, R. The improvement of a regional climate model by coupling a land surface model with eco-physiological processes: A case study in 1998. *Clim. Chang.* **2015**, *129*, 457–470. [\[CrossRef\]](#)
21. Ahlström, A.; Raupach, M.R.; Schurgers, G.; Smith, B.; Arneth, A.; Jung, M.; Reichstein, M.; Canadell, J.G.; Friedlingstein, P.; Jain, A.K.; et al. The dominant role of semi-arid ecosystems in the trend and variability of the land CO<sub>2</sub> sink. *Science* **2015**, *348*, 895–899. [\[CrossRef\]](#)
22. Bao, Q.; Lin, P.; Zhou, T.; Liu, Y.; Yu, Y.; Wu, G.; He, B.; He, J.; Li, L.; Li, J.; et al. The Flexible Global Ocean-Atmosphere-Land system model, Spectral Version 2: FGOALS-s2. *Adv. Atmos. Sci.* **2013**, *30*, 561–576. [\[CrossRef\]](#)
23. Grise, K.M.; Polvani, L.M. Understanding the Time Scales of the Tropospheric Circulation Response to Abrupt CO<sub>2</sub> Forcing in the Southern Hemisphere: Seasonality and the Role of the Stratosphere. *J. Clim.* **2017**, *30*, 8497–8515. [\[CrossRef\]](#)
24. Törnqvist, R.; Jarsjö, J.; Pietroni, J.; Bring, A.; Rogberg, P.; Asokan, S.M.; Destouni, G. Evolution of the hydro-climate system in the Lake Baikal basin. *J. Hydrol.* **2014**, *519*, 1953–1962. [\[CrossRef\]](#)
25. Ji, J.; Hu, Y. A simple land surface process model for use in climate study. *J. Meteorol. Res.* **1989**, *3*, 342–351.
26. Ji, J.; Huang, M.; Li, K. Prediction of carbon exchanges between China terrestrial ecosystem and atmosphere in 21st century. *Sci. China Ser. D-Earth Sci.* **2008**, *51*, 885–898. [\[CrossRef\]](#)
27. Wang, J.; Bao, Q.; Zeng, N.; Liu, Y.; Wu, G.; Ji, D. Earth System Model FGOALS-s2: Coupling a dynamic global vegetation and terrestrial carbon model with the physical climate system model. *Adv. Atmos. Sci.* **2013**, *30*, 1549–1559. [\[CrossRef\]](#)
28. Peng, J.; Dan, L. The Response of the Terrestrial Carbon Cycle Simulated by FGOALS-AVIM to Rising CO<sub>2</sub>. In *Flexible Global Ocean-Atmosphere-Land System Model*; Springer: Berlin/Heidelberg, Germany, 2014; pp. 393–403.
29. Oda, T.; Maksyutov, S.; Andres, R.J. The Open-source Data Inventory for Anthropogenic CO<sub>2</sub>, version 2016 (ODIAC2016): A global monthly fossil fuel CO<sub>2</sub> gridded emissions data product for tracer transport simulations and surface flux inversions. *Earth Syst. Sci. Data* **2018**, *10*, 87–107. [\[CrossRef\]](#)
30. Peng, J.; Wang, Y.; Houlton, B.Z.; Dan, L.; Pak, B.; Tang, X. Global Carbon Sequestration Is Highly Sensitive to Model-Based Formulations of Nitrogen Fixation. *Glob. Biogeochem. Cycles* **2020**, *34*, e2019GB006296. [\[CrossRef\]](#)
31. Peng, J.; Dan, L. Impacts of CO<sub>2</sub> concentration and climate change on the terrestrial carbon flux using six global climate-carbon coupled models. *Ecol. Model.* **2015**, *304*, 69–83. [\[CrossRef\]](#)
32. Peng, J.; Dan, L.; Yang, F.; Tang, X.; Wang, D. Global and regional estimation of carbon uptake using CMIP6 ESM compared with TRENDY ensembles at the centennial scale. *J. Geophys. Res. Atmos.* **2012**, *126*, e2021JD035135. [\[CrossRef\]](#)
33. Peng, J.; Peng, J.; Dan, L.; Ying, K.; Yang, S.; Tang, X.; Yang, F. China's Interannual Variability of Net Primary Production Is Dominated by the Central China Region. *J. Geophys. Res. Atmos.* **2021**, *126*, e2020JD033362. [\[CrossRef\]](#)
34. Sitch, S.; Friedlingstein, P.; Gruber, N.; Jones, S.D.; Murray-Tortarolo, G.; Ahlström, A.; Doney, S.C.; Graven, H.; Heinze, C.; Huntingford, C.; et al. Recent trends and drivers of regional sources and sinks of carbon dioxide. *Biogeosciences* **2015**, *12*, 653–679. [\[CrossRef\]](#)
35. Friedlingstein, P.; Friedlingstein, P.; O'sullivan, M.; Jones, M.W.; Andrew, R.M.; Hauck, J.; Olsen, A.; Peters, G.P.; Peters, W.; Pongratz, J.; et al. Global Carbon Budget 2020. *Earth Syst. Sci. Data* **2020**, *12*, 3269–3340. [\[CrossRef\]](#)
36. Zhang, X.; Rayner, P.; Wang, Y.; Silver, J.D.; Lu, X.; Pak, B.; Zheng, X. Linear and nonlinear effects of dominant drivers on the trends in global and regional land carbon uptake: 1959 to 2013. *Geophys. Res. Lett.* **2016**, *43*, 1607–1614. [\[CrossRef\]](#)
37. Piao, S.; Sitch, S.; Ciais, P.; Friedlingstein, P.; Peylin, P.; Wang, X.; Ahlström, A.; Anav, A.; Canadell, J.; Cong, N.; et al. Evaluation of terrestrial carbon cycle models for their response to climate variability and to CO<sub>2</sub> trends. *Glob. Chang. Biol.* **2013**, *19*, 2117–2132. [\[CrossRef\]](#)
38. Piao, S.; Ciais, P.; Friedlingstein, P.; de Noblet-Ducoudré, N.; Cadule, P.; Viovy, N.; Wang, T. Spatiotemporal patterns of terrestrial carbon cycle during the 20th century. *Glob. Biogeochem. Cycles* **2009**, *23*. [\[CrossRef\]](#)
39. Thornton, P.; Zimmermann, N. An Improved Canopy Integration Scheme for a Land Surface Model with Prognostic Canopy Structure. *J. Clim.* **2007**, *20*, 3902–3923. [\[CrossRef\]](#)
40. Zhao, M.; Heinsch, F.A.; Nemani, R.R.; Running, S.W. Improvements of the MODIS terrestrial gross and net primary production global data set. *Remote Sens. Environ.* **2005**, *95*, 164–176. [\[CrossRef\]](#)
41. Wieder, W.; Cleveland, C.C.; Smith, W.; Todd-Brown, K. Future productivity and carbon storage limited by terrestrial nutrient availability. *Nat. Geosci.* **2015**, *8*, 441–444. [\[CrossRef\]](#)
42. Loveland, T.R.; Reed, B.C.; Brown, J.F.; Ohlen, D.O.; Zhu, Z.; Yang, L.W.M.J.; Merchant, J.W. Development of a global land characteristics database and IGBP DISCover from 1 km AVHRR data. *Int. J. Remote Sens.* **2000**, *21*, 1303–1330. [\[CrossRef\]](#)
43. Fernández-Martínez, M.; Sardans, J.; Chevallier, F.; Ciais, P.; Obersteiner, M.; Vicca, S.; Canadell, J.G.; Bastos, A.; Friedlingstein, P.; Sitch, S.; et al. Global trends in carbon sinks and their relationships with CO<sub>2</sub> and temperature. *Nat. Clim. Chang.* **2019**, *9*, 73–79. [\[CrossRef\]](#)

- 
44. Piao, S.; Wang, X.; Park, T.; Chen, C.; Lian, X.; He, Y.; Bjerke, J.; Chen, A.; Ciais, P.; Tømmervik, H.; et al. Characteristics, drivers and feedbacks of global greening. *Nat. Rev. Earth Environ.* **2020**, *1*, 14–27. [[CrossRef](#)]
  45. Kim, I.-W.; Stuecker, M.F.; Timmermann, A.; Zeller, E.; Kug, J.-S.; Park, S.-W.; Kim, J.-S. Tropical Indo-Pacific SST influences on vegetation variability in eastern Africa. *Sci. Rep.* **2021**, *11*, 10462. [[CrossRef](#)] [[PubMed](#)]
  46. Mei, R.; Wang, G. Impact of Sea Surface Temperature and Soil Moisture on Summer Precipitation in the United States Based on Observational Data. *J. Hydrometeorol.* **2011**, *12*, 1086–1099. [[CrossRef](#)]
  47. Dai, A. Increasing drought under global warming in observations and models. *Nat. Clim. Chang.* **2013**, *3*, 52–58. [[CrossRef](#)]
  48. Meier, W.N.; Hovelsrud, G.K.; Van Oort, B.E.; Key, J.R.; Kovacs, K.M.; Michel, C.; Haas, C.; Granskog, M.; Gerland, S.; Perovich, D.K.; et al. Arctic sea ice in transformation: A review of recent observed changes and impacts on biology and human activity. *Rev. Geophys.* **2014**, *52*, 185–217. [[CrossRef](#)]
  49. Dai, A.; Luo, D.; Song, M.; Liu, J. Arctic amplification is caused by sea-ice loss under increasing CO<sub>2</sub>. *Nat. Commun.* **2019**, *10*, 121. [[CrossRef](#)]
  50. Cao, L.; Bala, G.; Caldeira, K.; Nemani, R.; Ban-Weiss, G. Importance of carbon dioxide physiological forcing to future climate change. *Proc. Natl. Acad. Sci. USA* **2010**, *107*, 9513–9518. [[CrossRef](#)]
  51. Swann, A.L.S.; Hoffman, F.M.; Koven, C.D.; Randerson, J.T. Plant responses to increasing CO<sub>2</sub> reduce estimates of climate impacts on drought severity. *Proc. Natl. Acad. Sci. USA* **2016**, *113*, 10019–10024. [[CrossRef](#)]